Brain & Development 44 (2022) 391–400

BRAIN & DEVELOPMENT
Official Journal of the Japanese Society of Child Neurology

www.elsevier.com/locate/braindev

Original article

Hypomyelinating spastic dyskinesia and ichthyosis caused by a homozygous splice site mutation leading to exon skipping in *ELOVL1*

Taiko Takahashi [a,1], Sevcan Mercan [b,2], Takayuki Sassa [a,3], Günseli Bayram Akçapınar [c,4], Kanay Yararbaş [d,5], Seda Süsgün [e,f,g,6], Sibel Aylin Uğur İşeri [e,7], Akio Kihara [a,8], Nihan Hande Akçakaya [h,i,9,*]

[a] *Hokkaido University, Faculty of Pharmaceutical Sciences, Laboratory of Biochemistry, Sapporo, Japan*
[b] *Kafkas University, Faculty of Engineering and Architecture, Department of Bioengineering, Kars, Turkey*
[c] *Acibadem MAA University, Institute of Health Sciences, Department of Medical Biotechnology, Istanbul, Turkey*
[d] *Demiroglu Bilim University, Faculty of Medicine, Department of Medical Genetics, Istanbul, Turkey*
[e] *Istanbul University, Aziz Sancar Institute of Experimental Medicine, Department of Genetics, Istanbul, Turkey*
[f] *Istanbul University, Graduate School of Health Sciences, Istanbul, Turkey*
[g] *Bezmialem Vakif University, Faculty of Medicine, Department of Medical Biology, Istanbul, Turkey*
[h] *Demiroglu Bilim University, Faculty of Medicine, Department of Neurology, Istanbul, Turkey*
[i] *Spastic Children's Foundation of Turkey, Cerebral Palsy Turkey, Istanbul, Turkey*

Received 2 October 2021; received in revised form 14 February 2022; accepted 14 March 2022

Abstract

Introduction: Next generation sequencing technologies allow detection of very rare pathogenic gene variants and uncover cerebral palsy. Herein, we describe two siblings with cerebral palsy due to *ELOVL1* splice site mutation in autosomal recessive manner. ELOVL1 catalyzes fatty acid elongation to produce very long-chain fatty acids (VLCFAs; ≥C21), most of which are components of sphingolipids such as ceramides and sphingomyelins. Ichthyotic keratoderma, spasticity, hypomyelination, and dysmorphic facies (MIM: 618527) stem from *ELOVL1* gene deficiency in human.

Methods: We have studied a consanguineous family with whole exome sequencing (WES) and performed in depth analysis of cryptic splicing on the molecular level using RNA. Comprehensive analysis of ceramides in the skin stratum corneum of patients using liquid chromatography-tandem mass spectrometry (LC–MS/MS). ELOVL1 protein structure was computationally modelled.

Results: The novel c.376-2A > G (ENST00000372458.8) homozygous variant in the affected siblings causes exon skipping. Comprehensive analysis of ceramides in the skin stratum corneum of patients using LC–MS/MS demonstrated significant shortening of fatty acid moieties and severe reduction in the levels of acylceramides.

* Corresponding author at: Demiroglu Bilim University, Faculty of Medicine, Department of Neurology, Istanbul, Turkey.
E-mail addresses: nihanhande.akcakaya@demiroglu.bilim.edu.tr, nhakcakaya@gmail.com (N.H. Akçakaya).
[1] ORCID: 0000-0002-0741-2476.
[2] ORCID: 0000-0003-1500-6854.
[3] ORCID: 0000-0003-3145-9829.
[4] ORCID: 0000-0002-6296-7415.
[5] ORCID: 0000-0002-5314-3406.
[6] ORCID: 0000-0001-9689-3111.
[7] ORCID: 0000-0002-5790-6853.
[8] ORCID: 0000-0001-5889-0788.
[9] ORCID: 0000-0001-8414-4017.

https://doi.org/10.1016/j.braindev.2022.03.003

Discussion: It has recently been shown that disease associated variants of *ELOVL1* segregate in an autosomal dominant manner. However, our study for the first time demonstrates an alternative autosomal recessive inheritance model for *ELOVL1*. In conclusion, we suggest that in ultra-rare diseases, being able to identify the inheritance patterns of the disease-associated gene or genes can be an important guide to identifying the molecular mechanism of genetic cerebral palsy.

Keywords: Ceramide; ELOVL1; Exon skipping; Autosomal recessive; Hypomyelinating; Ichthyosis; Cerebral palsy

1. Introduction

Very long-chain fatty acids (VLCFAs) contain 21 or more carbons (≥C21) and constitute a small part of the total amount of fatty acids in the cell. Although VLCFAs are less abundant than long-chain fatty acids (LCFAs; C11–C20), they have important functions that cannot be substituted by LCFAs. Different biological membranes require different chain-lengths and degrees of unsaturation of VLCFAs [1–4]. Saturated and monounsaturated C22–C24 VLCFAs are the components of sphingolipids (ceramides, sphingomyelins, glycosphingolipids, etc), whereas polyunsaturated VLCFAs such as docosahexaenoic acid (C22:6) are constituents of glycerophospholipids [3,4]. The mammalian fatty acid (FA) elongase family (**EL**ongation **O**f **VL**CFA; ELOVL1–7) proteins are responsible for the synthesis of VLCFAs. ELOVL1, 5, and 6 are expressed ubiquitously, and rest of the others (ELOVL2, 3, 4, and 7) are tissue specific [5]. ELOVL1 primarily catalyzes the elongation of C20–C24 saturated and monounsaturated VLCFAs [6]. Galactosylceramides are one of the most abundant lipids in myelin in the white matter and predominantly contain C22 and C24 VLCFAs, which are synthesized by ELOVL1 [3,4,7]. Therefore, ELOVL1 is essential for the nervous system [1,2,7].

The sphingolipid backbone ceramides are composed of a long-chain base and an FA. Ceramides with ≥C26 VLCFAs synthesized by ELOVL1 and ELOVL4 constitute the extracellular lipid lamellae in the epidermal stratum corneum (SC) and are essential for epidermal permeability barrier (skin barrier) [8–10]. In the SC, there are various ceramide classes differing in long-chain base and FA moieties [11]. Of these, the epidermis-specific ω-*O*-acylceramides (acylceramides) and protein-bound ceramides are especially important for skin barrier function. Acylceramides have a unique three hydrophobic chain structure, where an ω-hydroxy C28–C36 VLCFA is esterified with a linoleic acid. Some acylceramides are metabolized to protein-bound ceramides, which are covalently bound to the cornified envelope in corneocytes (enucleated dead keratinocytes in the SC) [11,12]. Protein-bound ceramides are considered to hold the extracellular lipid lamellae on the surface of corneocytes. Whole body knockout (KO) of *Elovl1* causes reduction in the amount of epidermal acylceramides to about a quarter, leading to neonatal lethality due to abnormal skin barrier in mice [10]. KO of *Elovl1* in tissues other than the epidermis causes dry eye and neurological phenotypes, such as startle epilepsy, hypomyelination in large-diameter axons in the corpus callosum, and poorer motor coordination [7,13]. In human *ELOVL1* heterozygous missense mutation (p.Ser165Phe) causes an ultra-rare skin (ichthyosis) and brain disease (OMIM 618527) [14,15], although the exact pathomechanism, whether it is caused by haploinsufficiency or gain of function, has not been known yet. In societies where rate of parental consanguinity is high, including Turkey, there is increased probability of observing ultra-rare diseases due to identical by descent inheritance of rare pathogenic variants from the carrier but unaffected parents. Herein, we aimed to elucidate the variation in molecular and pathophysiological aspects of ceramide composition in a consanguineous family from Turkey triggered by the by the pathogenic *ELOVL1* mutation, which was shown to be inherited recessively for the first time.

2. Material and Methods

2.1. Patients

Patient 1-a nine year old girl was evaluated in outpatient cerebral palsy center of Spastic Children's Foundation of Turkey due to her movement difficulties. She was born to unaffected parents who are first degree cousins. Her past medical history was indicative of delayed motor developmental milestones, which had been accompanied by tremor. Her head control could be possible by the age of nine months and she could sit independently at about 20 months of age. Her history as reported by her parents was indicative of head tremor with head control. The tremor accompanying voluntary movements had spread to the whole body in accordance with her motor development from upper to lower extremities. She could never walk independently due to her involuntary movements. Her mental development milestones were normal. Intermittent urinary incontinence was present. Parents also reported dry, scaly skin problems especially in the first years after her birth.

In her clinical examination, titubation and tremor were remarkable. She had phenotypic happy face with

wide forehead, down slanting palpebral fissures, tubular nose with anteverted nares, low-set ears, long philtrum, and thin upper limp (Supplementary Fig. S1). Cranial nerves were intact. She had horizontal high-frequency low-amplitude nystagmus and prominent cerebellar dysarthria. There was extremity ataxia and high amplitude, short lasting, arhythmic ataxic extremity tremor emerging throughout the body, which became more evident with movement (Supplementary Video). Deep tendon reflexes were brisk at the low extremities. Spontaneous extensor toes were present. Mild ichthyotic skin was present at her back and abdomen. There were dark, coarse hyperkeratotic skin at her knees (Supplementary Fig. S1). Spasticity at the lower extremities showed a slight progression in the last four years.

Patient 2 was the 5-year-old brother of the patient 1. He had a similar developmental history, phenotypic appearance and neurological symptoms with his older sister. (Supplementary Fig. S1). He also could never able to walk even with assistance due to more prominent pyramidal involvement and mild flexion contractures in his knees.

Both patients were screened for inborn errors of metabolism and mitochondrial disorders with the results being within normal limits. Motor and sensory nerve conduction studies were also normal. There was sensorineural hearing loss at high frequencies. In their brain MRI, there was cerebral and cerebellar hypomyelination (Fig. 1). The family had been recruited to this study upon receiving written informed consents from or for all family members in accordance with the Declaration of Helsinki. The study protocol was approved by ethics committees of Acibadem Mehmet Ali Aydinlar University (ATADEK 2019-15/9) and Hokkaido University (permit no. 2019-005).

2.2. Molecular genetic studies of ELOVL1

DNA isolation from peripheral blood was performed by using QIAamp DNA mini kit (Qiagen, Germany).

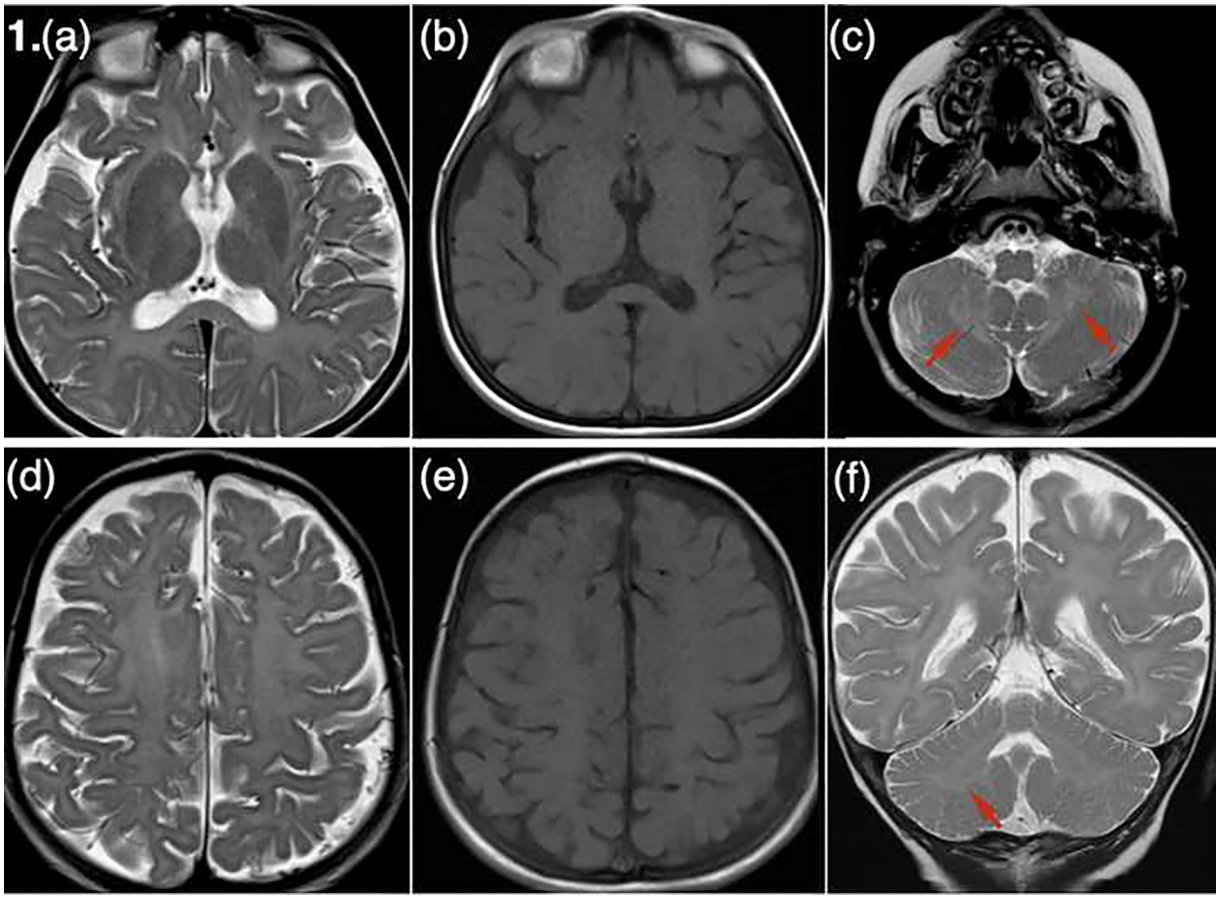

Fig. 1. Brain MRI findings of the patients. (a) T2-weighted axial image of the parent 1 shows diffuse white matter hyper-intensity at the age of six. Basal ganglias and thalami are seen relatively hypointense due to hypomylelination of the white matter. (b) T1-weighted axial image of the same section is nearly normal except delayed hyper-intensity in the white matter of the brain. (c) Cerebellar white matter hypo-intensities (red arrows) seen on T2-weighted axial image of the patient 1 at the age of six. (d) Diffuse white matter hypo-intensity at the level of centrum semiovale seen on T2 axial image of the patient 2 at the age of three. (e) T1-weighted axial image of the centrum semiovale section shows decreased hyper-intensity in the subcortical white matter broadly. (f) Coronal cerebellar T2-weighted brain image shows hypo-intensity due to hypomyelination of the corpus medullary (red arrow). (For interpretation of the references to color in this figure legend, the reader is referred to the web version of this article.)

Whole exome sequencing (WES) was performed for the affected sib pair. Exonic DNA was captured with the xGen® Exome Research Panel v1.0 and sequenced on the Illumina NovaSeq platform. Exome data analysis was completed using our in-house pipeline (https://github.com/AcuRARE/acugen). For recessive inheritance analysis, all shared rare variants with a carrier frequency expected for an ultra-rare recessive disorder (alternative allele frequency; AAF < 0.14%) were filtered [16]. For dominant inheritance model, all novel and shared variants were filtered. These variants were then re-annotated with ENSEMBL Variant Effector Predictor Tool (VEP) for both detecting the consequence of these variants on current transcript versions and retrieving up-to-date population frequency data. Sequence validation and segregation analyses were performed via Sanger sequencing for the determined variant using standard procedures.

For RNA based studies, RNA was isolated from fresh blood samples of all family members manually *via* the Trizol (Invitrogen) method. cDNA synthesis was performed by using random hexamers (Roche Diagnostics, Mannheim, Germany) and MMLV reverse transcriptase (MBI Fermentas, Lithuania) according to the manufacturer's protocol. Primer pairs residing on exon 4 (ENSE00003499131) and exon 7 (ENSE00003554824) of *ELOVL1* were designed to investigate the possibility of cryptic splicing. Resulting amplicons derived from cDNA were run on 2% agarose gels and Sanger sequenced to detect the effect of detected variant on ELOVL1 splicing.

For all *ELOVL1* based annotations the MANE select transcript (ENST00000372458.8; NM_022821.4) has been used.

2.3. Epidermal SC ceramide analyses

The SC samples were collected from the forearms of the patients and parents by tape stripping method, as described previously [17]. Each tape strip was subjected to lipid extraction, and ceramide and protein-bound ceramide species were measured through liquid chromatography–tandem mass spectrometry (LC–MS/MS), as described previously [17].

2.4. Computational modelling of ELOVL1

ELOVL1 protein structure was modelled via threading using the I-TASSER (Iterative Threading ASSEmbly Refinement) server [18]. Five models were generated, and best model was selected based on comparison of C-score, TM-Score, and cluster densities. Modelled protein structure was visualized with Visual Molecular Dynamics (VMD) software and compared to the crystal structure of human fatty acid elongase 7 (ELOVL7, PDB ID: 6Y7F) [19] as the closest and only homologue deposited in the PDB database [20]. Possible ligand binding sites/active site tunnels and tunnel forming residues within the modelled enzyme structure were predicted via Mole 2.0 and Caver3 tools [21,22].

3. Results

3.1. WES data analysis and detection of cryptic splicing in ELOVL1

As a first step in the WES analysis, shared and heterozygous variants were analyzed, as OMIM database reports autosomal dominant inheritance for *ELOVL1* variants associated with ichthyotic keratoderma, spasticity, hypomyelination, and dysmorphic facies (MIM: 618527). Then, WES data was examined for possible autosomal recessive candidate variants. These analyses revealed a shared, novel and homozygous splice acceptor variant in the fifth intron of *ELOVL1* composed of seven exons (ENST00000372458.8:c.376-2A > G). Segregation analysis with Sanger sequence both verified homozygosity in the patients and showed carrier status for the parents (Supplementary Figs. S2 and S3). The SpliceAI tool utilized through Ensembl-VEP predicted high confidence for both a potential splicing acceptor gain and loss effect for this variant [23]. Therefore, we have performed in depth analysis of cryptic splicing on the molecular level using RNA extracted from freshly obtained peripheral blood of all four family members. This analysis was suggestive for loss of exon 6 as detected both in agarose gel electrophoresis and Sanger sequencing providing evidence for splice acceptor loss (Fig. 2).

3.2. Epidermal ceramide analyses

To investigate the effect of the recessive *ELOVL1* mutation on VLCFA synthesis in the patients' epidermis, we comprehensively analyzed the SC ceramides by LC–MS/MS. There are five types of long-chain bases (dihydrosphingosine [DS], sphingosine [S], phytosphingosine [P], 6-hydroxy sphingosine [H], and 4,14-sphingadiene [SD]) and five types of FAs (non-hydroxy FA [N], α-hydroxy FA [A], ω-hydroxy FA [O], esterified ω-hydroxy FA [EO], and protein-bound ω-hydoxy FA [P-O]) that constitute human ceramides (Fig. 3a), resulting in 20 classes of non-protein-bound ceramides and 5 classes of protein-bound ceramides [11]. Each ceramide class is represented by a combination of long-chain base and FA abbreviations. All acylceramide classes (EOH, EOS, EOP, EODS, and EOSD) were greatly reduced in the patients' SCs compared to the parents (Fig. 3b and Supplementary Tables S1, S2). These lower quantities of acylceramides in the patients than in the parents were observed irrespective of FA chain-length (C26–C36), as shown in EOS

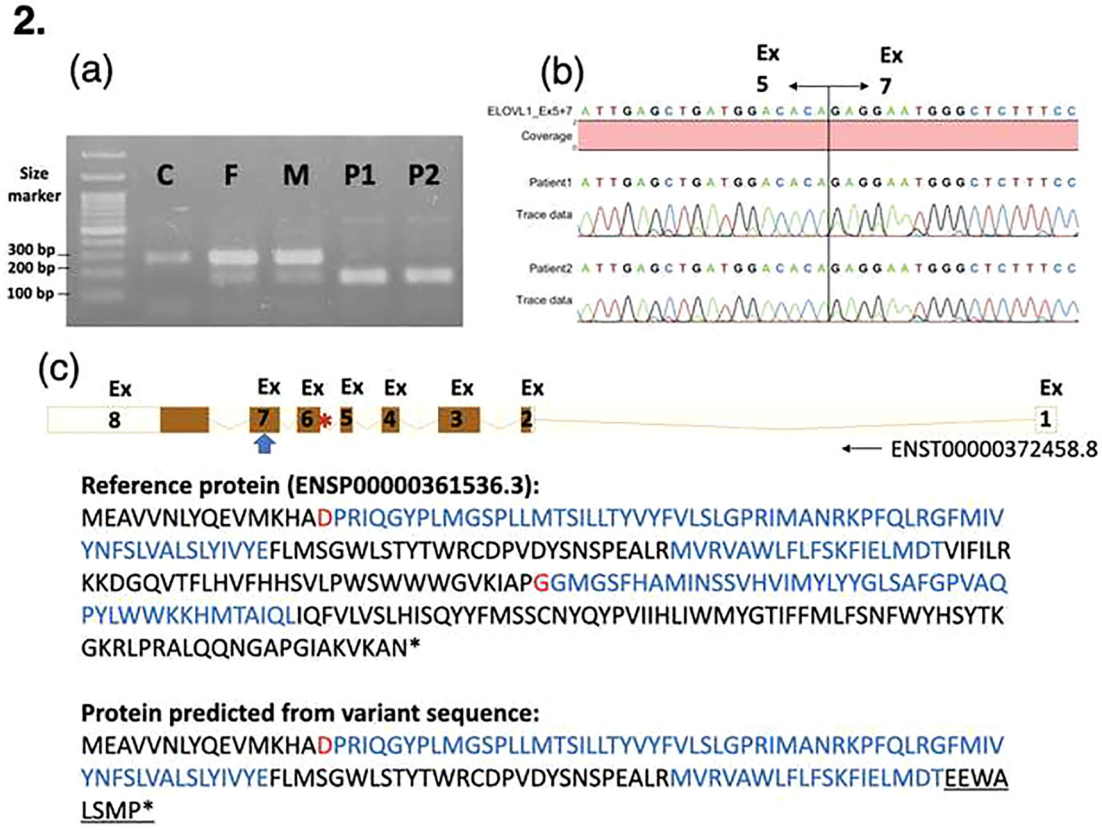

Fig. 2. (a) Agarose gel electrophoresis of amplicons derived via PCR of cDNAs obtained from family members and a control individual. Primers within exon 5 and 7 result in a PCR product of 279 base pairs (bp) in the control individual (C). Amplicons for both patients (P1 and P2) are shorter than expected, while there is heterozygosity for amplicons of parents (F and M). (b) The amplicon for each patient is Sanger sequenced which is indicative for the loss of exon 6 in cDNA samples. (c) The exon–intron structure of ELOVL1 (ENST00000372458.8) is shown schematically on the genome level (modified from Ensembl release 104 - May 2021). The position of the variation on the genome level is depicted with an asterisk. The early stop codon encoded in exon 7 due to cryptic splicing is marked with a blue arrow. The potential amino acid sequences of the reference protein (ENSP00000361536.3) and the predicted truncated protein of 133 amino acids are also given. Blue highlighting indicates alternating exons and red highlighting indicates amino acids encoded across a splice junction as in CCDS database. (For interpretation of the references to color in this figure legend, the reader is referred to the web version of this article.)

(Fig. 3c), for example. In contrast, the amounts of most non-acylated ceramides were similar between patients and parents (Fig. 3b). Exceptionally, the amounts of NH and ADS ceramides were slightly lower in patients than in the parents. When the total FA composition of non-protein-bound ceramide classes was compared between the parents and patients' SCs, ceramides with ≥C25 fatty acid were reduced and those with ≤C23 were increased (Fig. 3d), indicating that ELOVL1 is important for the elongation of fatty acids from C23/C24 to C25/C26 in the epidermis. In contrast to the large decreases in acylceramides, the quantities of protein-bound ceramide classes (P-OS, P-OH, P-OP, P-OSD, and P-ODS) were comparable between the parents and patients' SCs (Fig. 3e and Supplementary Tables S3, S4).

Fig. 3. Changes in ceramide profile in the patients' stratum corneum. (a) Structure and nomenclature of ceramides. Shown are the structures of fatty acids (left), long-chain bases (middle), and NDS ceramide (upper right). Nomenclature of 25 ceramide classes (lower right), comprising 20 classes of non-protein-bound ceramides (with N, A, O, or EO type fatty acid moiety) and 5 classes of protein-bound ceramides (with P-O type fatty acid moiety). Each ceramide class is represented as a combination of the abbreviations corresponding to its fatty acid and long-chain base moieties. Typically, "n" is 1–9 for ceramides with N or A type fatty acid moiety (total carbon chain-length; 16–24) and 13–21 for those with O, EO, or P-O type (total carbon chain-length; 28–36). (b–e) Stratum corneum samples were collected from two patients and their parents by tape stripping method. From each tape strip, lipids were extracted and subjected to ceramide measurement through liquid chromatography–tandem mass spectrometry. (b) Quantity of each non-protein-bound ceramide class. Inset is an enlarged graph of 5 EO type ceramides (acylceramides). (c) Fatty acid composition of EOS class. (d) Total fatty acid composition of non-protein-bound ceramide classes. Each bar is the sum of saturated and monounsaturated fatty acids with the indicated chain-length. (e) Quantity of each protein-bound ceramide class. Values represent means ± SD. Significant differences from the parents are indicated (** $p < 0.01$; * $p < 0.05$; Student's *t*-test). Data for all ceramides measured are provided in Supplementary Tables S1–S4.

3.3. Computational modelling of truncated ELOVL1

The splice-site mutation was predicted to affect splicing both by *in silico* tools and functional analysis of patient derived cDNA samples. Based on these points, we have investigated that the homozygous splice site mutation through a mutant transcript in the blood tissue within the family. The loss of exon 6 causes a shorter

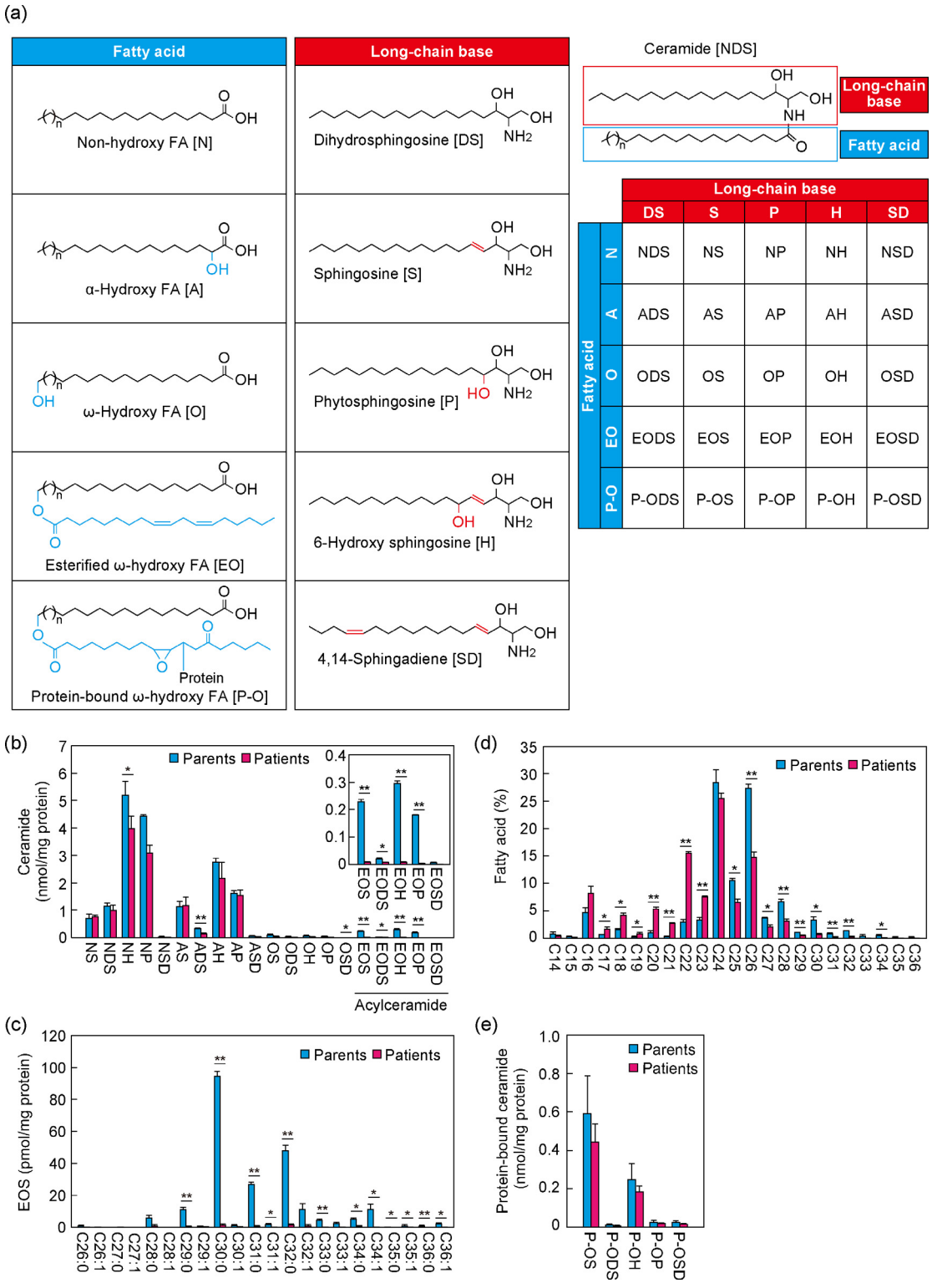

protein product with the loss of 154 amino acids and an addition of 8 new amino acids to the C terminus instead. Effect of the splice site mutation on the protein structure and function was further analyzed via computational modelling of the ELOVL1 protein. I-TASSER was used to model the protein structure. The closest and only homologue of the ELOVL1 with a determined 3D structure was ELOVL7 (PDB ID: 6Y7F) [19]. I-TASSER predicted the best model with a C-score of 0.52, a TM-score of 0.78 ± 0.09. Structural alignment of ELOVL7 with ELOVL1 were shown in Fig. 4a with the OFN (~{S}-[2-[3-[[(2~{R})-4-[[[(2~{R},3~{S},4~{R},5~{R})-5-(6-aminopurin-9-yl)-4-oxidanyl-3-phosphonooxy-oxolan-2-yl]methoxy-oxidanyl-phosphoryl]oxy-oxidanyl-phosphoryl]oxy-3,3-dimethyl-2-oxidanyl-butanoyl]amino]propanoylamino]ethyl] 3-oxidanylidene-icosanethioate) ligand from 6Y7F to indicate the structural similarity of both proteins. Ribbon and surface representation models of the ELOVL1 structure were exhibited in Fig. 4b and 4c, respectively. Deleted residues of ELOVL1 was shown in red color and OFN obtained from the ELOVL7 (PDB ID: 6Y7F) structure was shown in blue color with ELOVL1 in order to project the possible ligand binding sites. The splice site mutation results in loss of the transmembrane helices in close proximity to the active site tunnel, essentially covering the active site thereby forming a possibly non-functional enzyme even if folded properly (Fig. 4d and 4e). Ligand tunnel and cavity analysis with Mole 2.0 and CAVER3 indicated possible active site tunnels in ELOVL1. CAVER server predicts three main tunnels whereas MOLE server predicts twenty tunnels. Fig. 5a shows three tunnels and tunnel bottleneck forming residues. Fig. 5b exhibits the longest predicted tunnel (59 Å long) as predicted by MOLE server. Residues between 125 and 279 were located in the vicinity of these predicted tunnels and cavities by both programs (Fig. 5a, 5b).

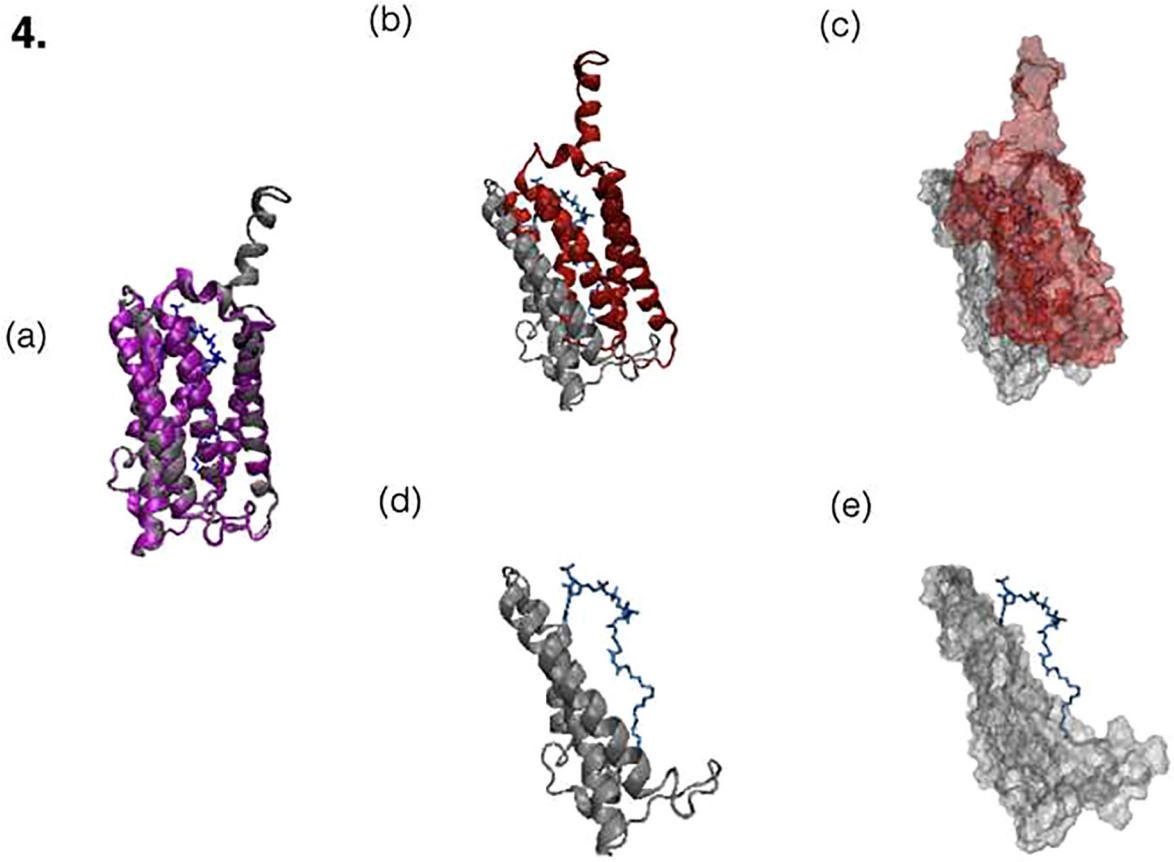

Fig. 4. a) Structural alignment of modelled ELOVL1 structure with ELOVL7 (PDB ID: 6Y7F) structure. b) Ribbon representation models of the ELOVL1 structure c) Surface representation models of the ELOVL1 structure. All structural representations prepared with VMD. Red: Deleted amino acids, Blue: OFN (~{S}-[2-[3-[[(2~{R})-4-[[[(2~{R},3~{S},4~{R},5~{R})-5-(6-aminopurin-9-yl)-4-oxidanyl-3-phosphonooxy-oxolan-2-yl]methoxy-oxidanyl-phosphoryl]oxy-oxidanyl-phosphoryl]oxy-3,3-dimethyl-2-oxidanyl-butanoyl]amino]propanoylamino]ethyl] 3-oxidanylidene-icosanethioate) ligand obtained from the ELOVL7 (PDB ID: 6Y7F) structure with ELOVL1. d) Ribbon e) surface representation models of ELOVL1 without the deleted amino acids with the OFN substrate. (For interpretation of the references to color in this figure legend, the reader is referred to the web version of this article.)

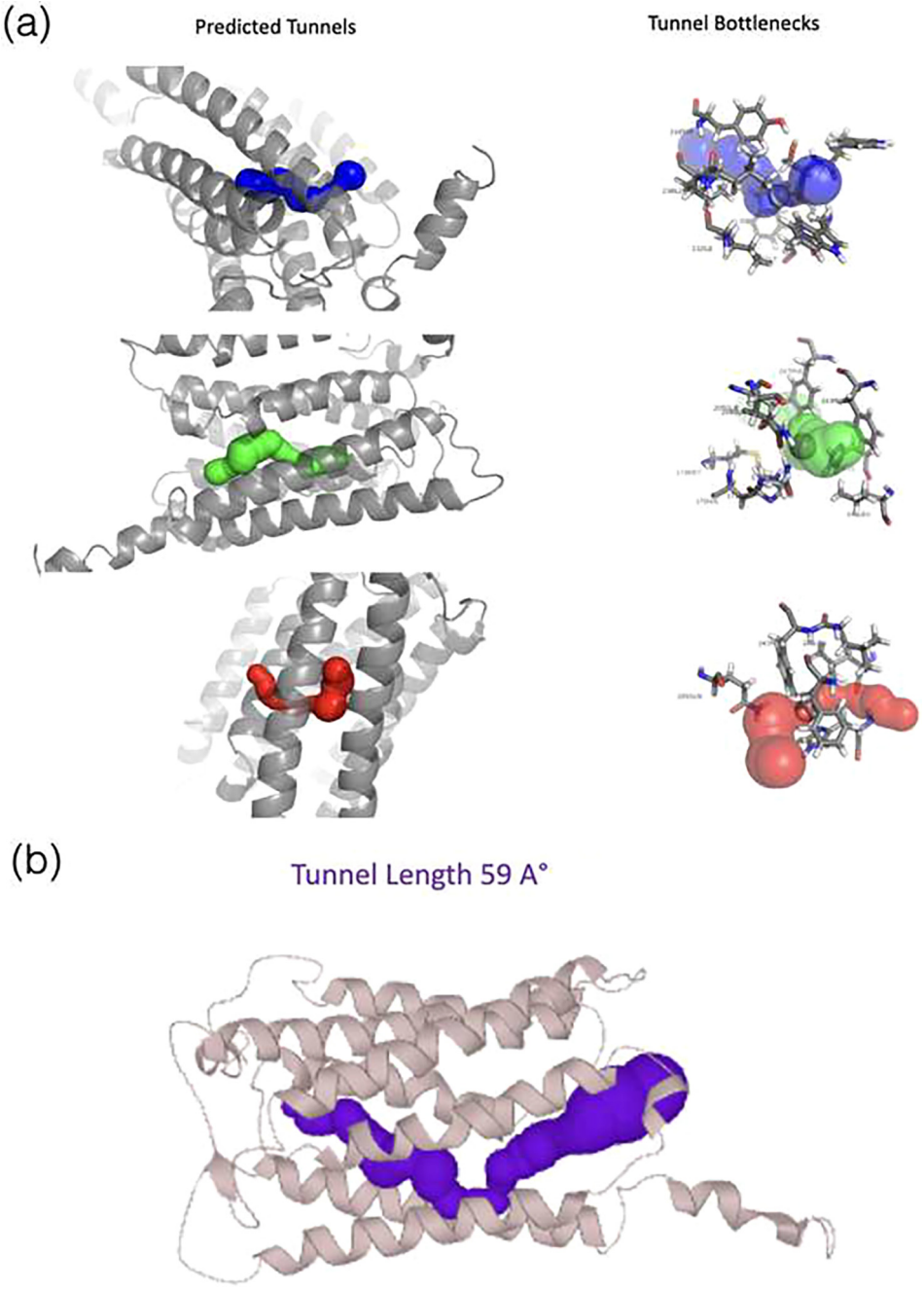

Fig. 5. a) Ligand binding tunnel predictions by CAVER. CAVER predicted 3 tunnels indicated with blue, green and red colors. Residues forming the tunnel bottlenecks are shown on the right b) Longest ligand binding tunnel prediction by MOLE server. Purple: longest ligand binding tunnel predicted. (For interpretation of the references to color in this figure legend, the reader is referred to the web version of this article.)

4. Discussion

Previously skin symptoms and spasticity weighted neurological involvement secondary to central hypomyelination due to *ELOVL1* mutation with autosomal dominant inheritance pattern in two families has been described [14,15]. Here, we report for the first time involvement of a homozygous *ELOVL1* splice site mutation, which causes the similar symptoms to the previous one. Mainly skin findings and central nervous system hypomyelination in our patients with the absence of peripheral nerve involvement, hearing loss at high frequencies, and pale viewing of the optic discs are the similar features. However, the central nervous system hypomyelination of the patients appears as diffuse cerebral and partially involves the cerebellum.

Hypomyelination involving the whole cerebral hemispheres and in the cerebellar white matter areas shows more widespread and prominent involvement than the previously reported patients (Fig. 1). The hypomyelina-

tion did not change in the 2-year MRI follow-up. Cerebellar involvement is localized in corpus medullare in both patients. Findings in the neurological phenotype that occur in the patients show correlation with the hypomyelination observed in the brain MRI. This cerebellar corpus medullare hypomyelination correlates with extremity ataxia neuroanatomically, which is the main cause of disability in patients. In *Elovl1* KO mice, FA moieties in brain sphingolipids including galactosylceramides, which are one of the most abundant myelin lipids, were significantly shortened: predominantly C22–C24 in wild type but C18–C20 in *Elovl1* KO mice [7]. The similar changes in myelin lipids may occur in the patients and associated with their neurological phenotypes.

Although *ELOVL1* exhibits a ubiquitous expression pattern, epidermal involvement and central nervous system hypomyelination dominantly from birth indicates tissue specific tolerability of its gene defects. The patients' ichthyosis symptoms and lethal phenotype of KO animal model indicate that *ELOVL1* is extremely vital for skin barrier formation. In the patients' SCs, acylceramides were nearly absent (Fig. 3), which suggests that this reduction is likely responsible for the pathogenesis of ichthyosis. On the other hand, the levels of protein-bound ceramides, which are produced from acylceramides and also essential for the skin permeability barrier formation, little changed in the patients' SC. Although this lack of correlation between acylceramides and protein-bound ceramides is unusual, the same observation was reported in an ichthyosis patient with a hypomorphic mutation in the epidermis-specific ceramide synthase gene *CERS3* [24] and in mouse model with gene disruption of the acyl-CoA synthetase *Fatp4* [25]. The decrease in the levels of acylceramides may disturb the structure of lipid lamellae, which causes the residual acylceramides to diffuse more freely from the lipid lamellae to the surface of corneocytes, where they are converted to protein-bound ceramides until the surface of corneocytes is fully covered by protein-bound ceramides.

The splice-site variant predicted to affect splicing by *in silico* tools was functionally shown to produced cryptic splicing by removing exon 6 via our in depth RNA-based studies. This loss of exon 6 possibly creates a premature stop codon (PTC) on the RNA level producing a truncated protein of 134 amino acids. It is speculative if this PTC activates nonsense mediated decay mechanism or not as this PTC should potentially reside on the 7th exon, which is the penultimate one. Transcripts with PTCs on the last or penultimate exons may escape nonsense mediated decay mechanism and be translated into truncated protein products [26]. We therefore further studied the effect of this possible truncation on the protein structure and function *via* computational modelling of the ELOVL1 protein.

The homozygous c.376-2A > G found in this study and the previously reported heterozygous c.494C > T (p.Ser165Phe) mutation [14,15] leads to reduction in > C24 VLCFAs. The effect of the homozygous recessive mutations on the VLCFA production seems stronger than that of the dominant heterozygous mutation. Accordingly, the neurological findings in our patients are more severe and early onset than those in patients with a dominant mutation. The molecular pathophysiology is unknown in the dominant inheritance. The enzymatic activity of the dominant, p.Ser165Phe mutant protein is severely reduced [15], which may suggest the haploinsufficiency. However, the parents harboring a heterozygous c.376-2A > G mutation exhibit no skin and neurological phenotypes, which suggests that the dominant mutation is not a simple loss of function but takes on the characteristics of gain of function. Skin findings and central nervous system hypomyelination are the key findings for ELOVL1 gene pathology that compatible with life.

5. Ethics

Ethical approvals for the study were obtained from the local ethics committee of Acıbadem MAA University (ATADEK 2019-15/9) and from the ethics committee of Hokkaido University (permit no. 2019-005). The photos and videos of patients were used upon obtaining a second written consent.

Conflict of Interest

The authors declare no competing interests.

Acknowledgement

This work was supported by KAKENHI Grant Numbers JP18H03876 (to A.K.) and JP19K07060 (to T.S.). We also thank to Turkish Academy of Sciences for the 2019 Distinguished Young Scientist Award to SAUI.

Appendix A. Supplementary data

Supplementary data to this article can be found online at https://doi.org/10.1016/j.braindev.2022.03.003.

References

[1] Becker I, Wang-Eckhardt L, Yaghootfam A, Gieselmann V, Eckhardt M. Differential expression of (dihydro)ceramide synthases in mouse brain: oligodendrocyte-specific expression of CerS2/Lass2. Histochem Cell Biol 2008;29(2):233–41.

[2] Imgrund S, Hartmann D, Farwanah H, Eckhardt M, Sandhoff R, Degen J, et al. Adult ceramide synthase 2 (CERS2)-deficient mice

exhibit myelin sheath defects, cerebellar degeneration, and hepatocarcinomas. J Biol Chem 2009;284(48):33549–60.
[3] Kihara A. Very long-chain fatty acids: elongation, physiology and related disorders. J Biochem 2012;152(5):387–95.
[4] Sassa T, Kihara A. Metabolism of very long-chain fatty acids: genes and pathophysiology. Biomol Ther 2014;22(2):83–92.
[5] Guillou H, Zadravec D, Martin PGP, Jacobsson A. The key roles of elongases and desaturases in mammalian fatty acid metabolism: Insights from transgenic mice. Prog Lipid Res 2010;49(2):186–99.
[6] Ohno Y, Suto S, Yamanaka M, Mizutani Y, Mitsutake S, Igarashi Y, et al. ELOVL1 production of C24 acyl-CoAs is linked to C24 sphingolipid synthesis. Proc Natl Acad Sci U S A 2010;107(43):18439–44.
[7] Isokawa M, Sassa T, Hattori S, Miyakawa T, Kihara A. Reduced chain length in myelin sphingolipids and poorer motor coordination in mice deficient in the fatty acid elongase *Elovl1*. FASEB Bioadv 2019;1(12):747–59.
[8] Cameron DJ, Tong Z, Yang Z, Kaminoh J, Kamiyah S, Chen H, *et al.* Essential role of Elovl4 in very long chain fatty acid synthesis, skin permeability barrier function, and neonatal survival. Int J Biol Sci. 2007;3(2):111–119.
[9] Vasireddy V, Uchida Y, Salem N Jr, Kim SY, Mandal MN, Reddy GB, *et al.* Loss of functional ELOVL4 depletes very long-chain fatty acids (≥C28) and the unique ω-O-acylceramides in skin leading to neonatal death. Hum Mol Genet. 2007;16(5):471–482.
[10] Sassa T, Ohno Y, Suzuki S, Nomura T, Nishioka C, Kashiwagi T, et al. Impaired epidermal permeability barrier in mice lacking *Elovl1*, the gene responsible for very-long-chain fatty acid production. Mol Cell Biol 2013;33(14):2787–96.
[11] Kihara A. Synthesis and degradation pathways, functions, and pathology of ceramides and epidermal acylceramides. Prog Lipid Res 2016;63:50–69.
[12] Muñoz-Garcia A, Thomas CP, Keeney DS, Zheng Y, Brash AR. The importance of the lipoxygenase-hepoxilin pathway in the mammalian epidermal barrier. Biochim Biophys Acta 2014;1841(3):401–8.
[13] Sassa T, Tadaki M, Kiyonari H, Kihara A. Very long-chain tear film lipids produced by fatty acid elongase ELOVL1 prevent dry eye disease in mice. FASEB J 2018;32(6):2966–78.
[14] Kutkowska-Kaźmierczak A, Rydzanicz M, Chlebowski A, Kłosowska-Kosicka K, Mika A, Gruchota J, et al. Dominant *ELOVL1* mutation causes neurological disorder with ichthyotic keratoderma, spasticity, hypomyelination and dysmorphic features. J Med Genet 2018;55(6):408–14.
[15] Mueller N, Sassa T, Morales-Gonzalez S, Schneider J, Salchow DJ, Seelow D, et al. *De novo* mutation in *ELOVL1* causes ichthyosis, *acanthosis nigricans*, hypomyelination, spastic paraplegia, high frequency deafness and optic atrophy. J Med Genet 2019;56(3):164–75.
[16] Hennekam RC. Care for patients with ultra-rare disorders. Eur J Med Genet 2011;54(3):220–4.
[17] Kawana M, Miyamoto M, Ohno Y, Kihara A. Comparative profiling and comprehensive quantification of stratum corneum ceramides in humans and mice by LC/MS/MS. J Lipid Res 2020;61(6):884–95.
[18] Zhang Y. I-TASSER server for protein 3D structure prediction. BMC Bioinf 2018;9:40.
[19] Nie L, Pascoa TC, Pike ACW, Bushell SR, Quigley A, Ruda GF, et al. The structural basis of fatty acid elongation by the ELOVL elongases. Nat Struct Mol Biol 2021;28(6):512–20.
[20] Humphrey W, Dalke A, Schulten K. VMD: visual molecular dynamics. J Mol Graph 1996;14(1):33–8.
[21] Chovancova E, Pavelka A, Benes P, Strnad O, Brezovsky J, Kozlikova B, *et. al.* CAVER 3.0: a tool for the analysis of transport pathways in dynamic protein structures. PLoS Comput Biol. 2012;8(10):e1002708.
[22] Sehnal D, Svobodová Vařeková R, Berka K, Pravda L, Navrátilová V, Banáš P, et al. MOLE 2.0: advanced approach for analysis of biomacromolecular channels. J Cheminform 2013;5(1):39.
[23] Jaganathan K, Kyriazopoulou Panagiotopoulou S, McRae JF, Darbandi SF, Knowles D, Li YI, et al. Predicting splicing from primary sequence with deep learning. Cell 2019;176(3):535–548.e24.
[24] Yamamoto M, Sassa T, Kyono Y, Uemura H, Kugo M, Hayashi H, et al. Comprehensive stratum corneum ceramide profiling reveals reduced acylceramides in ichthyosis patient with *CERS3* mutations. J Dermatol 2021;48(4):447–56.
[25] Yamamoto H, Hattori M, Chamulitrat W, Ohno Y, Kihara A. Skin permeability barrier formation by the ichthyosis-causative gene *FATP4* through formation of the barrier lipid ω-*O*-acylceramide. Proc Natl Acad Sci U S A 2020;117(6):2914–22.
[26] Coban-Akdemir Z, White JJ, Song X, Jhangiani SN, Fatih JM, Gambin T, et al. Identifying genes whose mutant transcripts cause dominant disease traits by potential gain-of-function alleles. Am J Hum Genet 2018;103(2):171–87.